

# State Space Models Naturally Produce Time Cell and Oscillatory Behaviors and Scale to Abstract Cognitive Functions

Sen Lu\*, Xiaoyu Zhang\*, Mingtao Hu, Eric Yeu-Jer Lee, Soohyeon Kim, Wei D. Lu<sup>#</sup>

Electrical Engineering and Computing Science, University of Michigan

\*Both authors contributed equally

# Corresponding Email: [wluuee@umich.edu](mailto:wluuee@umich.edu)

## Abstract

A grand challenge in modern neuroscience is to bridge the gap between the detailed mapping of microscale neural circuits and mechanistic understanding of cognitive functions. While extensive knowledge exists about neuronal connectivity and biophysics, how these low-level phenomena eventually produce abstract behaviors remains largely unresolved. Here, we propose that a framework based on State Space Models, an emerging class of deep learning architectures, can help bridge this gap. We suggest that the differential equations governing elements in a State Space Model are conceptually consistent with the dynamics of biophysical processes, while the model offers a scalable framework to build on the dynamics to produce emergent behaviors observed in experimental neuroscience. We test this framework by training a model employing a diagonal state transition matrix on temporal discrimination tasks with reinforcement learning. Our results suggest that neural behaviors such as time cells naturally emerge from two fundamental principles: optimal pre-configuration and rotational dynamics. These features are shown mathematically to optimize history compression, and naturally generate structured temporal dynamics even prior to training, mirroring recent findings in biological circuits. We show that learning acts primarily as a selection mechanism that fine-tunes these pre-configured oscillatory modes, rather than constructing temporal codes *de novo*. The model can be readily scaled to abstract cognitive functions such as event counting, supporting the use of State Space Models as a computationally tractable framework for understanding neural activities.

## Introduction

The last few decades have witnessed extraordinary progress in neuroscience, particularly in mapping the brain's intricate wiring diagram. We can now trace pathways with synaptic resolution and record the activity of thousands of neurons simultaneously during complex behaviors<sup>1,2</sup>. Yet, questions still remain on how the collective activity of these meticulously mapped circuits gives rise to cognitive functions such as memory, perception, or the recognition of an abstract concept<sup>3</sup>.

Among these cognitive functions, the ability to perceive and judge temporal intervals is particularly fundamental<sup>4</sup>. Within experimental neuroscience, a key discovery is the existence of 'time cells'<sup>5</sup>, neurons found in regions including the hippocampus, prefrontal cortex, and striatum<sup>6</sup>. These cells become active sequentially, each firing at a specific moment during a timed delay period<sup>7</sup>. Together, their activity effectively marks the flow of time. Alongside

these, researchers have identified other properties, such as ‘ramping cells’, whose firing rates monotonically increase or decrease over a timed interval<sup>8</sup>, and persistent neural oscillations, which are also thought to be critical for time-keeping<sup>9</sup>. These discoveries offer a powerful insight into the neural basis of temporal memory, but they also raise deeper questions: What are the underlying mechanisms of these temporal codes? What is the role of learning vs. innate structures given recent observations that these sequences can flexibly recalibrate, or ‘remap’, to adapt to different durations without re-training? A model that can provide theoretical insight into these questions remains a key objective in the field.

In the effort to model phenomena like time cells, prevailing approaches have often operated from two opposing perspectives. Approaches from the bottom-up start from the neuron. At the microscale, since detailed biophysical models like the Hodgkin–Huxley model (HH model)<sup>10</sup> provide an exquisite description of how action potentials are generated based on the dynamics of ion channels. These models are grounded in molecular processes but are computationally intensive and difficult to scale into large networks capable of cognitive tasks<sup>11,12</sup>. On the other hand, the top-down approach utilizes concepts of neural networks such as recurrent neural networks (RNNs)<sup>13</sup>, convolutional neural networks (CNNs)<sup>14</sup> and transformer-based Large Language Models (LLMs)<sup>15</sup>, to describe cognitive processes. Studies using artificial neural networks to support neuroscience findings have recently moved beyond phenomenological reproduction, demonstrating that time-cell-like sequences, ramps, and oscillations may naturally emerge in RNNs and Deep Reinforcement Learning (DRL) agents trained on timing and working memory tasks<sup>16,17</sup>. For example, Lin et al.<sup>17</sup> established that these dynamics are not merely by-products of training but actively support value estimation and policy computation, with time and ramping cells carrying decodable information about temporal intervals and stimulus identity. Similarly, work by Zhou et al.<sup>16</sup> has shown that trained RNNs can generate realistic spiking sequences akin to biological time cells. However, while these models confirm that temporal codes can emerge from recurrent activity, they often lack an explanation for why biological circuits favor specific representations over others. Additionally, time cells exhibit complex adaptive behaviors beyond what are typically expressible through simple recurrent models. While some neural circuits rescale or stretch their temporal receptive fields, others exhibit remapping. For instance, Taxidis et al.<sup>18</sup> demonstrated that hippocampal time-cell ensembles remap rather than stretch when delays are extended in working memory tasks.

Recent lines of evidence also challenge the assumption that temporally organized sequences are exclusively the product of learning from scratch<sup>19</sup>, pointing instead to the critical role of preconfigured, intrinsic network architectures. While the Entorhinal Cortex (EC) is often believed to be the driver of downstream temporal codes, Heys and Dombeck<sup>20</sup> imply that CA1 and CA3 networks possess an inherent capacity to generate sequential firing dynamics even when EC input is compromised, although these intrinsic sequences display reduced stability. This suggests that the fundamental machinery for temporal organization resides within the local circuit dynamics themselves. Expanding on this view, van der Molen et al.<sup>21</sup> recently reported the emergence of preconfigured neuronal firing sequences in the human brain, systems entirely devoid of sensory experience. Together, these findings suggest that

temporal processing may not require *de novo* learning but rather exploits pre-existing, intrinsic dynamics that are biologically hardwired into the neural microcircuitry.

Here we propose that state space models (SSMs), originally developed in the field of control theory and recently used as a generative model for sequence processing<sup>22,23</sup>, can bridge the millisecond time scale, microscale neuronal behaviors with the long-time scale, macroscale functions. In particular, we show that the model, through pre-configured structural basis, can naturally produce desired neural behaviors such as time cells and oscillations even without learning. Learning primarily helps choose specific compressed history states for a given task, rather than constructing temporal codes *de novo*.

Unlike standard RNNs that operate in discrete steps, SSMs are rooted in continuous-time differential equations, making them conceptually isomorphic to biophysical models of neuronal dynamics. In this view, a neuron's internal state—encompassing membrane potential and ion channel kinetics—is a continuous vector that evolves based on its history and external inputs. Formally, a linear time-invariant SSM is governed by:

$$h'(t) = Ah(t) + Bx(t), \quad (1)$$

$$y(t) = Ch(t), \quad (2)$$

where,  $h(t) \in \mathbb{C}^N$  is the hidden state,  $x(t) \in R^M$  is the input,  $y(t) \in R^P$  is the output,  $A, B$ , and  $C$  are learnable parameters. Matrix  $A$  and  $B$  govern the state's evolution and its response to input.

Recent theoretical advances demonstrate that initializing  $A$  according to the HiPPO framework (High-order Polynomial Projection Operators) optimally projects continuous history onto basis functions of orthogonal Legendre polynomials<sup>24</sup>. Here we adopt a diagonalized version of this approach with complex-valued coefficients<sup>25</sup>, denoted as  $\Lambda$ . For computational implementation, this continuous system is discretized with a step size  $\Delta t$ , yielding the recurrence:

$$h(t + \Delta t) = \bar{\Lambda}(\Delta t)h(t) + \bar{B}x(t + \Delta t), \quad (3)$$

where  $\bar{\Lambda}(\Delta t) = \exp(\Lambda \Delta t)$  and  $\bar{B} = \Lambda^{-1}(\exp(\Lambda) - I)B$ . Due to the diagonal structure of  $\bar{\Lambda}$ , individual state evolves independently following a rotational dynamics before being mixed at the readout layer.

This mathematical formulation leads to our central premise: these optimal pre-configured oscillatory states act as a structural basis for temporal cognition, and SSM offers the mathematical framework that leverages these dynamics as computational primitives. As conceptualized in Figure 1, the proposed approach explains the role of time cells and other temporal codes as basis functions for input compression, and explains their origins through rotational dynamics governed by equation (1). Incoming sensory streams, such as those from the EC, are projected onto these basis functions in the hippocampal network, the output of which are then used for downstream tasks.

Importantly, we show that temporal receptive fields can be obtained from optimal initialization rather than training, i.e., models initialized according to the HiPPO framework<sup>26</sup> spontaneously exhibit time-cell sequences and ramping activity even before training. This result supports recent neurophysiological findings in the human brain organoid, where

backbone firing sequences emerge intrinsically from a preconfigured 3D neural architecture, independent of sensory experience<sup>21</sup>. In contrast, we found that randomly initialized networks fail to produce such structured dynamics even after extensive training. We suggest that optimal initialization serve as innate structural priors, a pre-configured architecture enabling neural systems to rapidly capture long-range temporal dependencies without the cost of learning.<sup>27</sup> From an evolutionary perspective, these findings support the argument that the brain's neural circuits may have been optimized during evolution to approximate these basis functions, allowing organisms to efficiently encode the complex temporal histories essential for survival. Learning is reinterpreted as a process of selection: mapping the sensory inputs to the basis functions and choosing specific compressed history states for downstream tasks, as schematically shown in Figure 1, while the basis functions themselves remain largely unchanged.

We then extend this mechanism to abstract cognitive functions, showing that continuous state-space trajectories can naturally transform repeating sensory inputs into decodable states, such as the event count. Collectively, these findings suggest that optimal state-space dynamics provide a computationally tractable and scalable framework for understanding of temporal cognition.

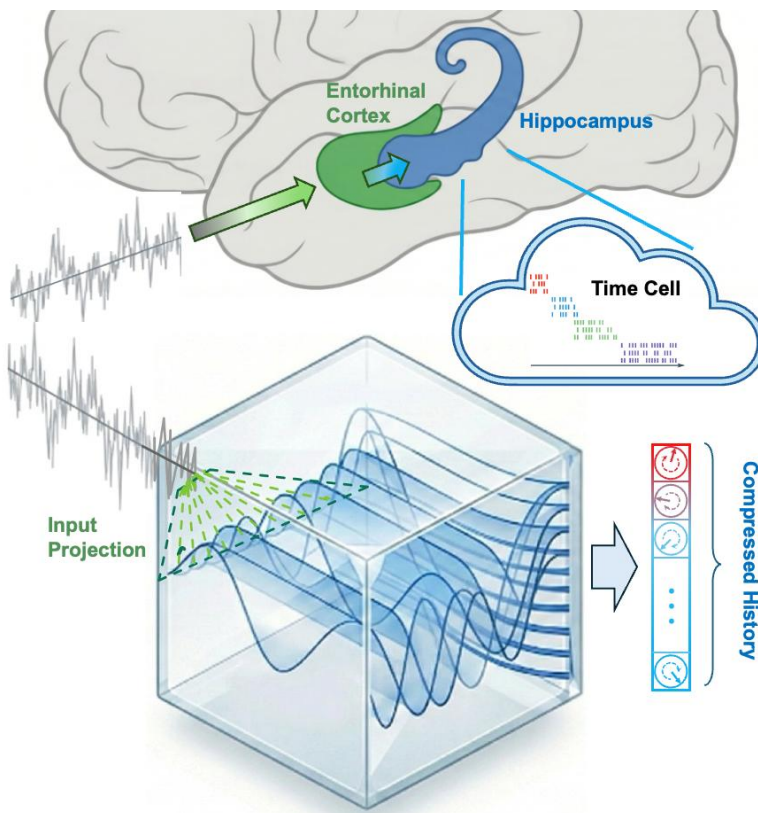


Figure 1 | A state-space perspective on neural temporal sequences. Top: sensory inputs (e.g., from the Entorhinal Cortex) are processed by intrinsic, pre-configured circuit dynamics manifested as time cells that naturally compress input history. Synaptic plasticity then acts as a selection mechanism, sampling from this dynamic basis to form specific temporal codes. Bottom: Mathematical implementation via an SSM. The HiPPO initialization serves as the mathematical proxy for the pre-configured structures, projecting continuous inputs onto a set of optimal orthogonal basis functions (visualized as trajectories within the cube). The

temporal information is compressed in a state vector, from which the network learns to select specific features for downstream tasks.

## Results

To test our hypothesis that pre-configured basis functions naturally lead to time cell behaviors, we trained an S5-based<sup>25</sup> agent on a temporal discrimination task using actor-critic deep reinforcement learning (Supplementary Information S3.1). As depicted in Fig. 2a, the agent's goal is to correctly identify the longest of three stimuli presented sequentially. The agent is trained through RL, similar to Lin et al.<sup>17</sup>, who utilized a Long Short-Term Memory (LSTM) module and trained the agents using the Asynchronous Advantage Actor-Critic (A3C) algorithm<sup>22</sup> to identify the longer sequence of two stimuli. In the three-stimuli case in our study, in addition to the final reward for the correct choice, the learning process is guided by rewarding the agent for choosing the longer of the first two stimuli (Supplementary Information S3.3). This intermediate reward aligns with the discovery that midbrain dopamine influences the perception of time in neurons<sup>28</sup>. The SSM layer output is then processed by the value network, which predicts the expected reward at the current state, and a policy network that predicts the action needed to be taken. Notably, the SSM layer communicates with the downstream policy and value networks through spiking signals, mimicking real neuron communication. A spike is generated from a hidden state unit when the real part of its activation value crosses a set threshold, analogous to a biological neuron's firing mechanism. After training, the agent can correctly identify the longest sequence with an accuracy of 86.5%.

We visualize the model's internal dynamics of the model by showing its states. Fig. 2b displays heatmaps of the real part of the state activities during the delays, averaged across 1000 trial episodes, during the two delay periods between the 3 stimuli. A clear sequential cascade emerges when these state units are sorted by the time of their peak activation, following Lin et al.<sup>17</sup>. Different units become selectively active at different moments, effectively cascading the entire temporal interval, replicating the time cell sequences observed in brain regions like the hippocampus and prefrontal cortex<sup>7</sup>. The heatmap also reveals high-frequency patterns in the remaining population (bottom rows). These higher-frequency dynamics are an inherent characteristic of the HiPPO-based initialization in diagonal SSMs, which theoretically necessitates eigenvalues with large imaginary components to optimally approximate history<sup>29</sup>. Since the internal state dynamics (Matrix  $\Lambda$  and  $B$ , see in Fig. 3c) remain largely stable during training, these high-frequency modes are preserved as basis functions, although we focus here on the lower-frequency components that manifest as explicit time cells. The sorting of the state space into low-frequency time and high-frequency cells applies to all tasks presented and the details can be found in Method section.

Furthermore, this single, unified architecture spontaneously produced a diverse set of temporal-coding mechanisms. Across the two delay periods, we found that about 20% of the population emerged as time cells, while about 60% exhibited monotonically increasing or decreasing activity (ramping cells), as illustrated by the example tuning curves in Fig. 2c. All

unsorted tuning curves are shown in Supplementary Information S2 and the specific criteria used to classify these distinct functional cell types are also detailed in the Methods section.

In essence, since the proposed S5 model uses a diagonal state matrix  $\Lambda$ , the state update during the delay  $h(t + 1) = \bar{\Lambda}h(t)$  simplifies to a set of independent equations for each state element:  $h_i(t + 1) = \bar{\lambda}_i \times h_i(t)$ . Here,  $\lambda_i$ s are the diagonal elements of the discretized state matrix  $\Lambda$ , which are learnable complex parameters. During the delays, where information must be preserved without decay, the network learns values of  $\bar{\lambda}_i$  with a modulus of 1. Mathematically, this operation is a pure rotation in the complex plane and effectively performs a spectral decomposition of the network dynamics, treating them as independent latent oscillatory states<sup>30</sup>. This perspective aligns with the neural manifold hypothesis<sup>31</sup>, which posits that the collective activity of neural populations is governed by low-dimensional latent dynamics, and that individual neurons act as specific projections of these latent states<sup>32</sup>. Fig. 2d illustrates this unifying mechanism in which the diverse temporal profiles are simply projections of these underlying rotations onto the real axis. Within this framework, a time cell and a ramping cell are not distinct biological entities but rather manifestations of the different phases of rotational process projected onto axes. A state rotating at a specific frequency will appear as a time cell if its trajectory crosses the positive real axis during the delay. However, if it rotates from the positive real axis to the negative real axis or in the opposite direction, it reproduces the ramping cell behavior.

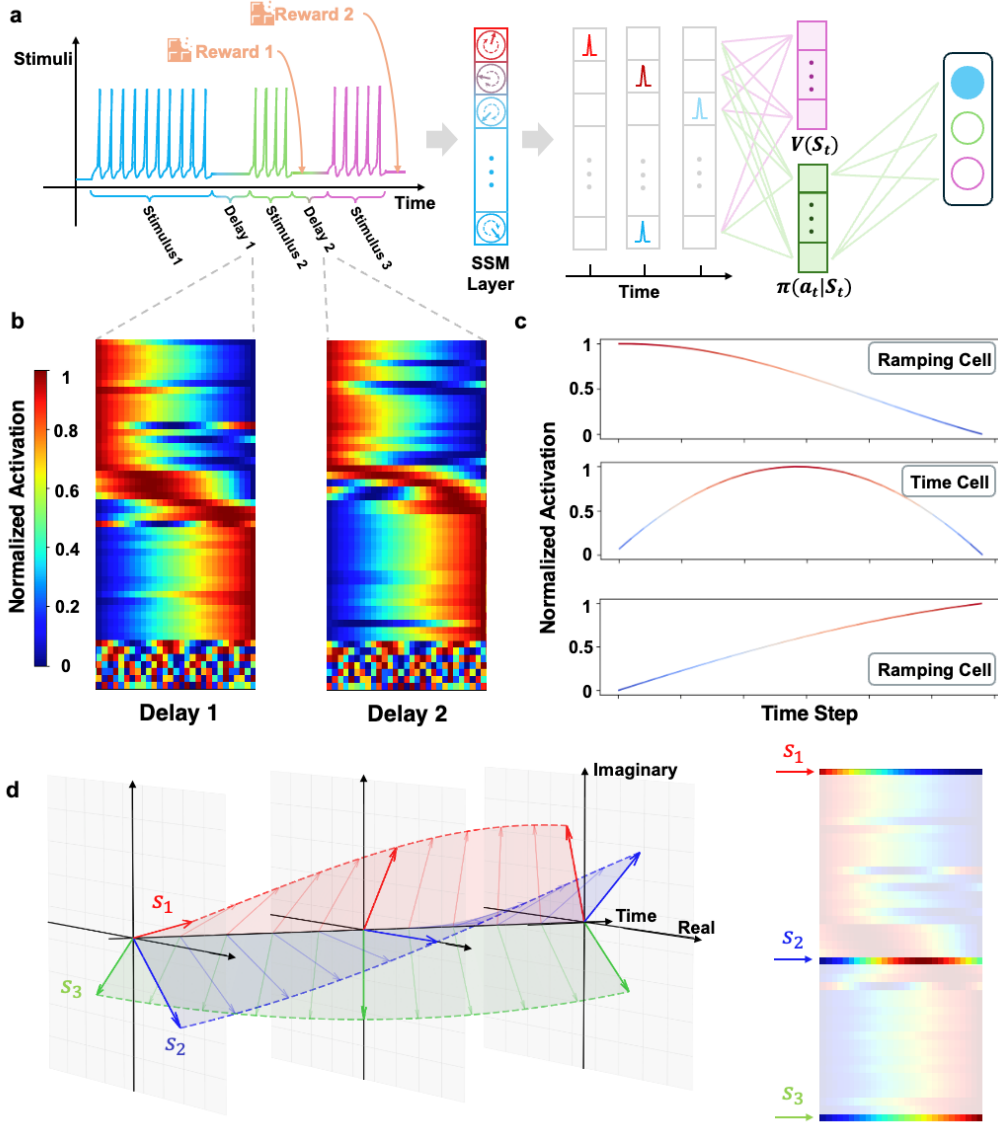


Figure 2 | Complex rotational dynamics naturally generate time cell behaviors in SSM. **a**, Learning Framework for the Temporal Judgment Task. The SSM layer processes three stimuli separated by two delay periods and is trained via reinforcement learning, with intermediate and final rewards, to identify the longest stimulus. On the right, the schematic illustrates the downstream readout architecture: continuous hidden states from the SSM layer are thresholded into discrete spiking signals. These spikes are then linearly projected to value network ( $V(S_t)$ ) and policy network ( $\pi(a_t|S_t)$ ). **b**, Emergent Time Cell behaviors during Delay Intervals. Heatmaps of trial-averaged, normalized state activations during the two delay periods reveal diverse temporal coding mechanisms, with a few of them highlighted in **c**. **c**, Example Tuning Curves of Individual State Units. Detailed activation profiles of representative units classified as ramping cells (ramping up and ramping down) and time cells. **d**, Unified View of Time and Ramping Cells. The diverse temporal profiles of states emerge from the projection of their rotational dynamics in the complex plane onto the real axis.

While the trained SSM exhibits sophisticated temporal dynamics driven by complex

rotations, a question remains regarding the origin of these representations: Are they constructed *de novo* through reinforcement learning, or do they arise from the network's intrinsic structure? To disentangle the contributions of structural inductive biases from learning-driven optimization, we compared the internal dynamics and performance of SSMs with HiPPO initialization versus random initialization.

As shown in Fig. 3a, both models can learn the task with high proficiency, achieving comparable accuracies. However, their underlying dynamic solutions differ fundamentally. Visualizing the hidden state activations reveals that the HiPPO-initialized model exhibits sequentially organized 'time cell' patterns even before training, a structure that is preserved and refined throughout the learning process without specifically training for it. This indicates that the HiPPO initialization equips the network with a set of 'preconfigured' basis functions capable of representing temporal history. This computational observation aligns with recent physiological findings in the human brain organoid, where structured 'backbone' firing sequences emerge intrinsically from neural architectures even without learning<sup>21</sup>. On the contrary, even after extensive training, a randomly initialized network only produced unstructured, high-entropy dynamics with no discernible temporal order (Fig. 3a, right), suggesting that the SSM architecture alone with pre-configured basis functions is insufficient to support stable sequential representations.

To demonstrate the mathematical mechanism underlying this dichotomy, we quantified the plasticity requirements of different network components during training. We tracked the relative change of the trainable parameters—the state transition matrix ( $\Lambda$ ), the input matrix ( $B$ ), and the readout matrix ( $C$ )—by computing the normalized distance between the initial and trained values ( $|\theta_{final} - \theta_{init}| / |\theta_{init}|$ ). As shown in Fig. 3b, a clear functional dissociation emerges between the internal dynamics and the readout layer. For the internal state parameters, the HiPPO-initialized model exhibits minimal change. The relative changes for  $\Lambda$  (mean  $\approx 0.37$ ) and  $B$  (mean  $\approx 0.83$ ) are significantly lower than those in the randomly initialized model ( $\Lambda$  mean  $\approx 1.60$ ;  $B$  mean  $\approx 2.16$ ). It is worth noting that the temporal nature of the tasks may lead the model to prefer temporally expressive initialization. Nevertheless, structural stability confirms that HiPPO initialization provides a near-optimal "encoder" structure in which the input information is compressed into the hidden state using preconfigured basis functions, requiring only minor fine-tuning rather than extensive restructuring.

In contrast, the readout matrix  $C$  evolves in the opposite way. Since both models initialize  $C$  randomly, they must learn to extract task-relevant information from the hidden states. However, the HiPPO-initialized model exhibits a substantially larger relative change in  $C$  (mean  $\approx 4.59$ ) compared to the randomly initialized model (mean  $\approx 2.75$ ). This suggests that in the HiPPO-initialized SSM training is largely through re-configuring connections of the basis functions to neurons in the downstream readout layer, while in random initialized models training involves significant updating of all parameters throughout the network. The latter case can still produce desired final outputs after aggressive training, but fails to explain the role of time cells observed in biology.

This structural hypothesis is further validated by the parameter-freezing experiment. Specifically, when we froze the internal parameters ( $\Lambda$  and  $B$ ) to their initial values and only trained the readout layer, the HiPPO-initialized model maintained an accuracy of 72.5%, whereas the random model's accuracy collapsed to approximately 53.1% under the same conditions. The random model failed to match the robust performance of the HiPPO model because its untrained internal dynamics cannot generate a useful state representation, and no amount of readout optimization can recover the lost information. Conversely, the HiPPO-initialized model's preconfigured structure effectively routes temporal information to the readout layer, proving that the emergence of time cells and task performance relies on the quality of the dynamic basis, not just the plasticity of the network.

These results support the hypothesis that time cells and other temporal codes are not merely artifacts of learning. Instead, evolutionary optimization could have created the necessary inductive bias to form orthogonal basis functions, manifested as HiPPO initialization in the SSM, that lead to the observed neural behaviors.

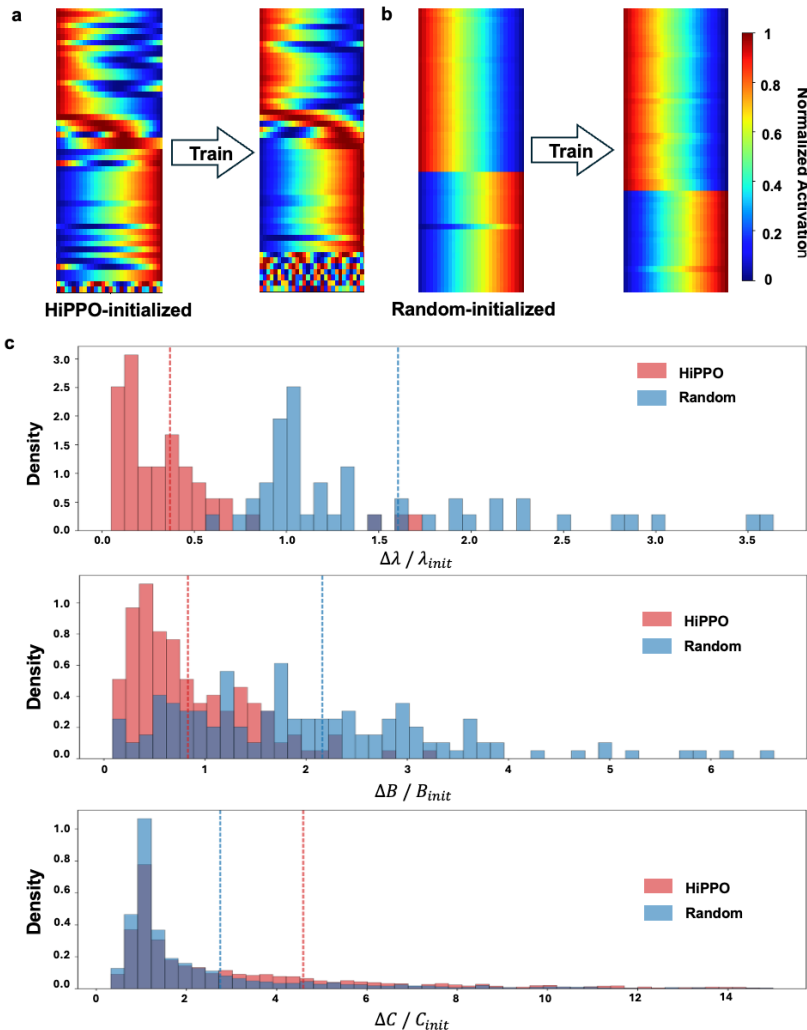


Figure 3 | Optimal initialization provides a robust structural basis, shifting the learning burden from internal dynamics to the readout layer. High frequency noises are removed for clearer presentation **a**, Intrinsic dynamics of untrained networks. Heatmaps of hidden state

activations show that HiPPO-initialization (left) generates time cell behaviors prior to training, whereas random initialization (right) produces unstructured noise. **b**, Quantification of parameter plasticity. Histograms showing the distribution of relative parameter changes ( $|\Delta \theta| / |\theta_{init}|$ ) after training with vertical dashed lines indicating the mean values. In the HiPPO-initialization model (red), the two parameters involved in the initialization ( $\Lambda$  and  $B$ ) exhibit minimal changes compared to the Random model (blue). For the output matrix  $C$ , the HiPPO-initialization model exhibits a larger relative change, demonstrating that the preconfigured state space allows the model to solve the task primarily by optimizing the downstream readout.

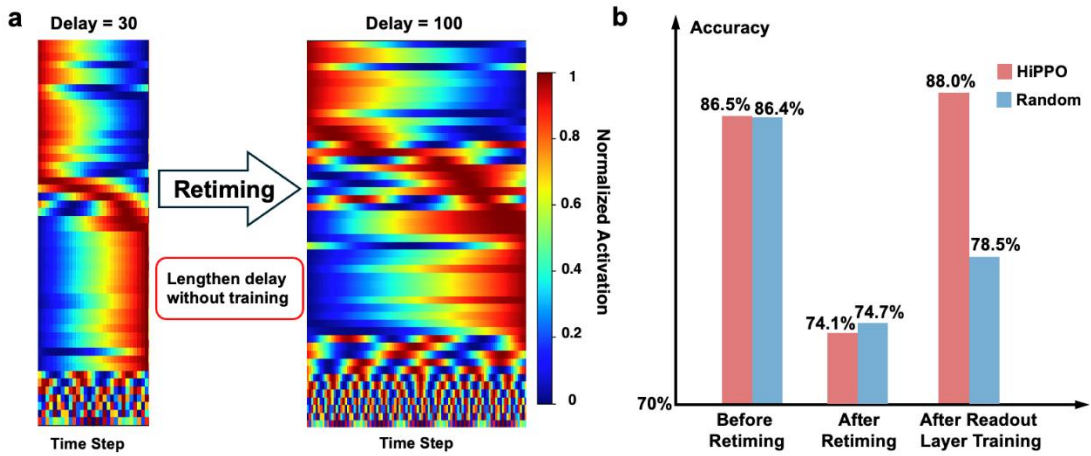


Figure 4 | Intrinsic Scalability of Temporal Representations. **a**, Heatmaps show that a model trained on a 30-step delay naturally produces stretched time-cell sequences when the delay is extended to 100 steps via retiming, even without retraining internal parameters. **b**, Divergent recovery of performance between initializations. While directly extending the delay causes a drop in accuracy, retraining only the linear readout layer (while keeping internal dynamics  $\Lambda$  and  $B$  frozen) fully restores the performance. In contrast, the randomly initialized model fails to adapt. Despite starting with comparable performance on the original task. This demonstrates that the learned oscillatory basis is robust and scalable, requiring only superficial re-calibration to adapt to new timescales.

To test whether the proposed framework captures biological adaptability, we performed a retiming experiment. Here, an agent originally trained on a short (30-step) delay was assessed on a significantly extended (100-step) interval without any retraining, to observe intrinsic scaling properties following Mello et al.<sup>33</sup>. The new internal state dynamics are shown in Fig. 4a, where we simply extended the delay period in the input stream while keeping all model parameters frozen at their values learned from the 30-step task. As evidenced by the heatmaps, the learned time-cell sequences did not fracture or reset; instead, the extended delay in the input allowed the pre-existing oscillatory modes to continue their respective rotations, with their projections on the real axis effectively tiling the entire 100-step interval. This test shows that the rotational dynamics offered by the basis functions in SSM offer a scalable temporal substrate, producing the intrinsic rescaling properties observed in biological circuits<sup>34</sup>. This behavior also mirrors the temporal scaling of invariant neural

trajectories reported in the primate medial frontal cortex, where the underlying dynamical structure is conserved across different speeds, allowing for the flexible production of varying intervals. We do note that the direct extension resulted in a misalignment between the stretched states and the readout layer, in which the accuracy dropped from 86.5% (for the original 30-step delay) to 74.1% after the delay was lengthened, as shown in Fig. 4b. Nonetheless, because the underlying temporal structure remained structurally intact (as seen in Fig. 4a), we hypothesized that the model only required a superficial recalibration. Indeed, by retraining only the readout-related layer while keeping the internal state dynamics ( $\Lambda$  and  $B$ ) completely frozen, the model's accuracy rapidly restored to 88.0% (Fig. 4b).

However, the retiming and recovery capabilities are unique to the structured initialization. We performed the same parameter-freezing experiment on the randomly initialized model. Although the randomly initialized model solved the original 30-step task with high accuracy (85.4%), its performance reduced to 74.7% for the extended delay and, unlike the HiPPO model, failed to recover after readout retraining, stagnating at 78.5% (Fig. 4b). These results further support the hypothesis that the optimally initialized SSM possesses necessary mechanisms to process time information that can be reused across timescales, matching what have been observed in biological systems.

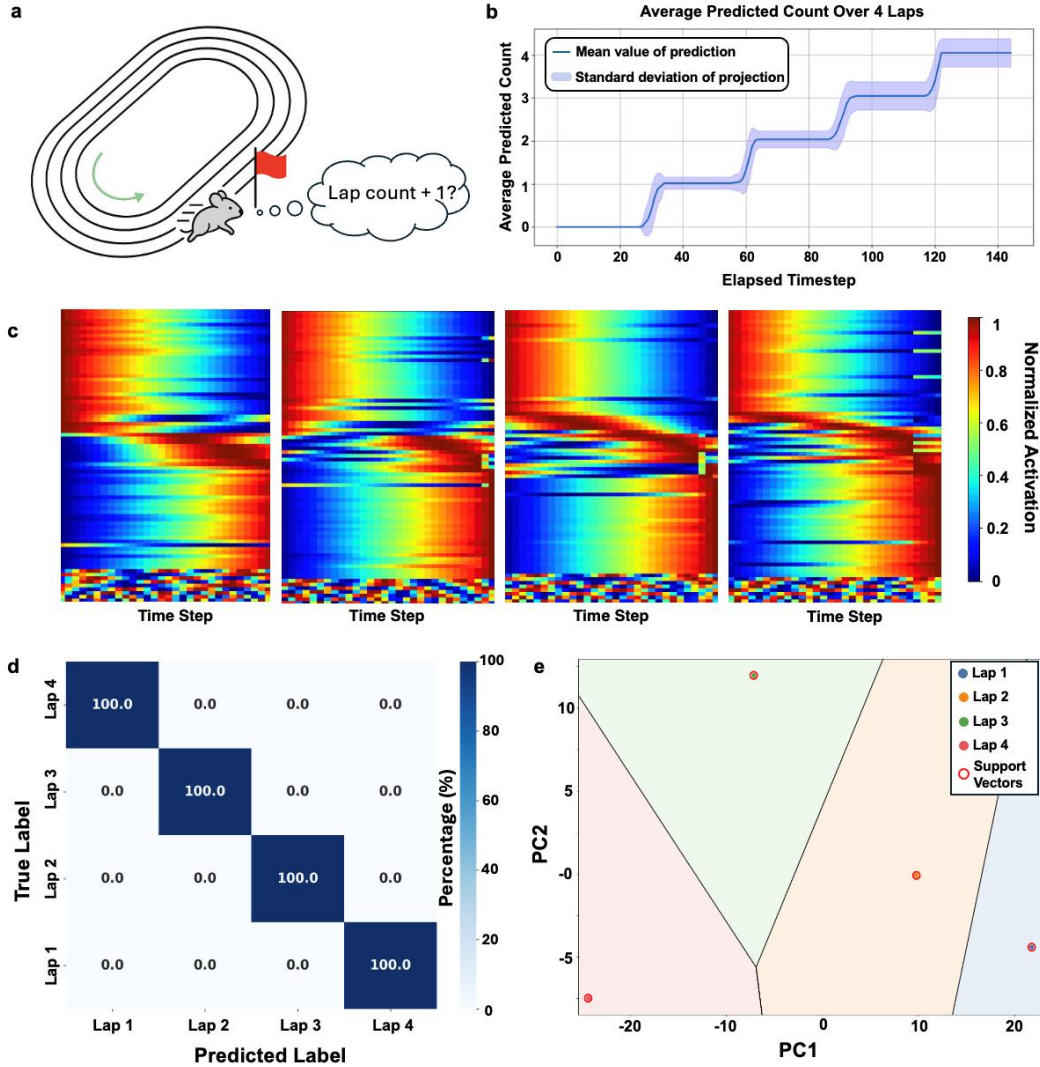


Figure 5 | Generalization of Temporal Coding to a Cyclical Lap-Counting Task **a**, Conceptual Diagram of the Lap-Counting Task. An agent processes a repeating sequence with a landmark and must learn to increment a counter after each ‘lap’. **b**, Accurate Lap-Counting Performance. The model’s average predicted lap count over time shows reliable, discrete increments at the end of each lap. **c**, Re-emergence of Time Cell Sequences Across Laps. The sequential activation of time cells resets and reliably replays during each consecutive lap.

Finally, we show that the same framework can be used to explain more abstract cognitive behaviors by simply connecting the internal SSM states to other downstream networks. To challenge the proposed model beyond simple interval timing and test the generality of the timing mechanism, we designed a more abstract lap-counting task. As conceptualized in Fig. 5a, the agent processes an input stream representing two alternating types of events: (1) A ‘running’ sequence, which represents the agent’s progress along the track. (2) A distinct ‘finish line’ landmark sequence. This experiment is inspired by the studies on mouse brains in Sun et al.<sup>35</sup>, where hippocampal neurons were found to represent discrete, repeated ‘lap events’ as fundamental units of an experience. The processing of such periodic sensory streams also parallels neurophysiological findings in the primate supplementary motor area (SMA) during rhythmic timing tasks<sup>36,37</sup>. In these tasks, neural populations generate periodic state-space trajectories that function as an internal clock to track repetitive intervals<sup>38</sup>.

As discussed in Sun et al.<sup>35</sup>, this is a much harder challenge for the agent as the agent must compress the temporal information of running (with identical sensory inputs in different laps) and specifically recognize the landmark sequence as the definitive cue to increment its internal lap count, demonstrating a move from simple timekeeping to abstract event recognition (detailed training description in Supplementary Information S3.4).

The model achieved 97.0% accuracy in terms of lap count against the random chance of  $P(X = 4) = C(140, 4) \cdot 0.5^4 \cdot (1 - 0.5)^{140-4} = 1.5 \times 10^7 \times 0.5^{140}$ , which is extremely small. However, it is also possible that the model correctly counted the laps at the incorrect timings. We therefore employed an edit distance metric that measures the dissimilarities between the predicted lap count timings and the ground truth timings to evaluate our model. This score is calculated by computing the cost of editing the predicted sequence to match the ground truth sequence. The proposed trained model achieved a normalized edit distance score (see Supplementary Information S4) of 0.94 (max at 1.0 for the exact same timings), showing extremely high alignments. Fig. 5b shows the model's average predicted lap count over four consecutive laps, each approximately 30-timestep long. The trace demonstrates a clear and accurate stepwise increment at the precise moment each lap ends, confirming the model's robust performance.

Similarly, the analysis of the hidden state dynamics indicates that the model naturally accomplished this through reward, without any explicit instructions regarding temporal coding. The heatmap in Fig. 5c visualizes the normalized activation of the hidden state units. Similar to Figs. 2-4, the units were sorted by their peak activation time independently within each of the four laps. The result shows a clear sequential cascade, the signature of time cell behavior, reliably re-emerged in every single lap (Fig. 5c). The intuitive question here is then: if the temporal firing patterns reset for each lap, how does the system maintain the persistent count information required to distinguish Lap 1 from Lap 2?

To investigate whether this abstract cognitive variable is explicitly represented in the neuronal dynamics, we performed a decoding analysis using a linear Support Vector Machine (SVM). We extracted the hidden state activity from the stable middle phase of each lap across 5,000 episodes. To test the robustness of the representation, we trained the classifier on a strictly limited subset of the data (only 10% for training) and evaluated it on the remaining 90% (4,500 episodes).

As shown in the confusion matrix in Fig. 5d, the linear classifier achieved 100% accuracy on the unseen test set. This perfect diagonal structure demonstrates that despite receiving identical sensory streams, the high-dimensional internal state for "Lap 1" is entirely distinct from "Lap 2". The fact that a linear classifier could solve this task with minimal training data implies that the abstract concept of "count" is not entangled in some complex manifold but is in fact linearly separable.

This geometric organization is visualized in Fig. 5e, where the decision boundaries are projected onto the first two principal components. The state space is partitioned into clear, distinct regions corresponding to each lap count. This finding is significant because it suggests that the HiPPO-initialized SSM naturally "unrolls" repetitive sensory inputs into a structured trajectory. The recurrent dynamics automatically segregate repeated events into distinct locations in the state space, allowing downstream readout layers to extract abstract variables—like event counts—via simple linear projections, without requiring additional non-linear processing.

## Discussion

Our results demonstrate that the emergence of sequential time cells in neural circuits is likely not an artifact of random connectivity or a learning process from scratch, but rather a manifestation of preconfigured innate strategies for compressing continuous history. By rigorously analyzing SSMs initialized with HiPPO dynamics, we propose a framework that bridges the gap between the millisecond timescale of cellular dynamics and the behavioral timescale of working memory. The rotational dynamics inherent to the HiPPO framework, which are necessary for orthogonal polynomial projection, manifest biologically as oscillatory behavior, suggesting that the brain's "intrinsic dynamics" may be physically instantiated implementations of these basis functions.

The HiPPO-initialized SSM utilizes a diagonal state transition matrix with complex-valued coefficients. This design is not merely a computational convenience, but appears to be grounded in biology. Studies on the reduction of the 4-dimensional Hodgkin-Huxley model demonstrate that while the system can be simplified, it cannot be reduced below two dimensions if it is to retain the capacity for oscillation (e.g., sub-threshold oscillations)<sup>39</sup>. A one-dimensional biophysical model is fundamentally over-damped and incapable of resonance. Our use of complex-valued states, which mathematically represent conjugate pairs of real variables, aligns with this irreducible two-dimensional requirement. These dynamics capture the minimal interplay between excitation and inhibition variables required for biological timekeeping. This biophysical necessity is paralleled at the systems level by evidence that voluntary motor timing relies on distributed neural trajectories within the pre-SMA and striatum. Such findings support the view that the rotational dynamics captured by the proposed model are intrinsic to the neural circuits governing temporal control<sup>40-42</sup>.

Several limitations of the current study still need to be addressed to fully contextualize these findings. First, the complexity of the tasks employed may not fully exploit the capacity of the proposed model framework. The fact that randomly initialized networks achieved relatively high accuracy suggests that the chosen tasks might be solvable with naïve designs, rather than requiring the robust, long-term history compression provided by HiPPO initialization. Second, while HiPPO represents a mathematically optimal solution for online function approximation, it is likely only one of a class of suitable initializations, and there is no biological guarantee that the brain utilizes this specific orthogonal basis over other potential pre-configured dynamics.

One potential future direction that these limitations point toward is a fertile intersection between control theory and evolutionary biology, such as the domain of meta-learning<sup>43,44</sup>. If evolution is viewed as a grand optimization process, the "intrinsic dynamics" observed in biological circuits could be interpreted as a meta-learned initialization. Future work should investigate whether evolving a population of SSMs over generations, selecting purely for memory capacity, causes weight matrices to spontaneously converge toward HiPPO-like structures, thereby validating the hypothesis that mathematical optimality is an attractor state for biological evolution. Finally, the current iteration of the proposed model relies on artificially encoded input signals, which simplifies the noisy nature of biological information

transmission. Since we have established a proof-of-concept linking continuous state-space dynamics to time cells, it will be critical to validate this framework using real spiking data, challenging the model to maintain robust historical representations amidst the sparsity and stochasticity inherent to actual neural substrates.

## Conclusion

In conclusion, our study suggests that the simple principle of rotational dynamics may be an essential computation for time perception. The SSM-based framework not only reproduces a wide array of biological observations within a single model but also provides a mathematical framework for generating hypotheses and understanding the algorithmic basis of cognition. This approach contributes to the ongoing effort to develop a multi-scale theory of how the brain learns to operate in time and offers a novel perspective on how neural circuits might function.

## Method

### Classification of Functional Cell Types

To characterize the temporal coding properties of hidden state units in the trained network, we analyzed their trial-averaged activity during the delay periods. Following successful training, we recorded the hidden state activations across 1,000 episodes with the network weights frozen. For each unit, we computed a trial-averaged temporal tuning curve. Based on the profile of this curve, units were classified into time cells and ramping cells.

Our criteria for identifying time cells and ramping cells were adapted from Shikano et al.<sup>45</sup>.

- **Ramping Cells:** A unit was classified as a ramping cell if its temporal tuning curve showed a monotonic increase or decrease. To quantify this, we fitted a linear regression to the tuning curve. A unit was considered a candidate ramping cell if the fit yielded a significant p-value ( $p \leq 0.05$ ) and a high Pearson correlation coefficient ( $\geq 0.9$ ).
- **Time Cells:** A unit was classified as a time cell if it fired selectively at a specific moment in the delay period. We identified these by calculating the temporal information of the tuning curve based on the Skaggs et al.<sup>46</sup> formula. If a unit was already a ramping candidate, its temporal information was calculated from the tuning curve after subtracting the linear regression fit to isolate peak-like activity from the ramp. A unit was considered a candidate time cell if its temporal information was significant (i.e., higher than the 99th percentile of a distribution generated from 100 shuffled tuning curves).

To ensure the temporal profiles were stable and not due to chance, all candidate ramping and time cells were subjected to a trial-reliability analysis. We computed a reliability score by correlating the tuning curves obtained from even- and odd-numbered trials. Only candidates with a significant reliability score (higher than the 99th percentile of scores from 100 shuffled comparisons) were confirmed as actual ramping or time cells. Note that these classifications were not mutually exclusive; a single unit could meet the criteria for multiple categories.

### Sorting Into Heatmaps

Given the broad frequency spectrum inherent to HiPPO initialization, we applied a two-stage sorting algorithm to isolate task-relevant temporal features for visualization. First, raw state trajectories were range-normalized and categorized by their oscillatory frequency, defined as the count of local maxima exceeding a specific amplitude prominence threshold. Second, within each frequency group, units were ordered by peak latency. Notably, units displaying one or two peaks were aggregated into a single cluster to account for boundary effects, where low-frequency 'time cells' may exhibit high values at both temporal edges. Implementation details are provided in the code repository.

### Actor-Critic RL Framework

Our framework, inspired by the design of Lin et al.<sup>17</sup>, employs an actor-critic architecture with an SSM memory module. The SSM processes the raw input signal stream to generate a state representation, which is fed to both the actor and critic networks.

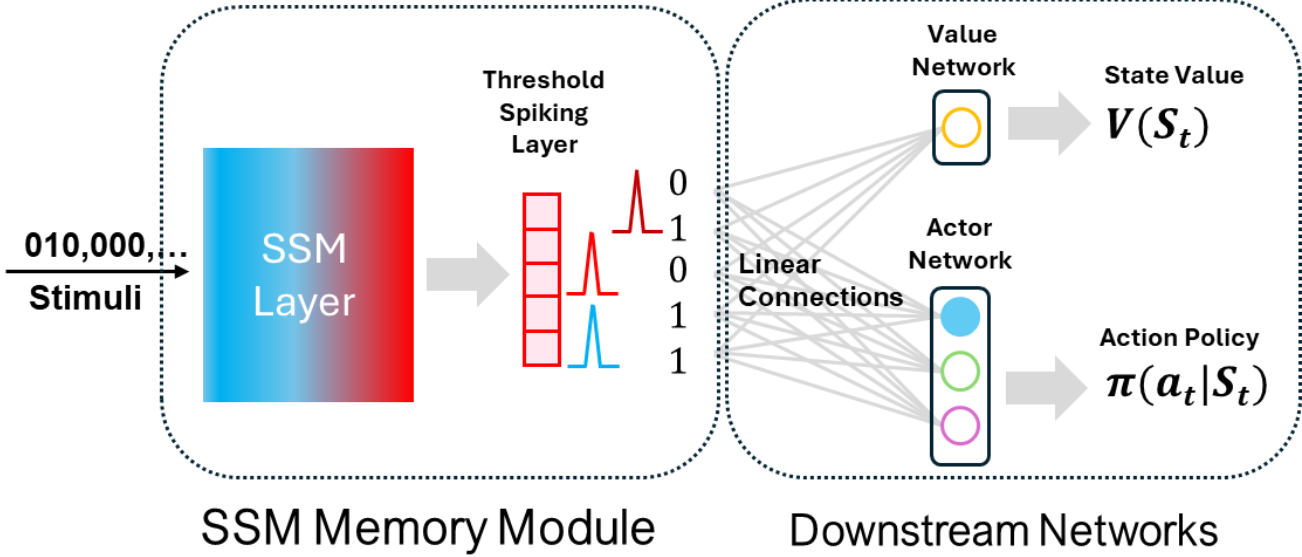


Figure 5: The overall architecture of the DRL agent. It includes an SSM layer and a threshold spiking layer that decodes hidden states into spikes. The spikes are then fed into downstream networks through linear connections to generate state value and action policy, respectively.

The actor-critic architecture is a widely used framework in reinforcement learning<sup>22</sup> that integrates both policy-based and value-based methods. It consists of two components: an actor that learns a policy to select actions based on the current state, and a critic that estimates a value function to evaluate the quality of actions or states. The agent was trained to minimize the loss of the policy and value networks,  $L = L_\pi + L_V$ , where

$$L_\pi = \sum_{t=0}^{T-1} -\log \pi * (R_t - \hat{V})$$

$$L_V = \sum_{t=0}^{T-1} l_1(\hat{V}, R_t)$$

where,  $T$  is the total timesteps of the trial in the episode, and  $R_t = \sum_{i=0}^t \gamma^i r_{t-i}$  is the reward computed at time  $t$  based on past reward,  $\gamma$  is the discount factor (set to 0.99 for all experiments), and  $l_1(\cdot)$  is the smoothed L1 loss.

The critic network, implemented as a linear layer, estimates the scalar state value,  $\hat{V}(S_t, \theta)$ . The actor network, also a linear layer, outputs a policy,  $\pi(a_t | S_t, \theta)$ , which is a probability distribution over the action space. A discrete action is then sampled from this distribution using a Softmax function with a temperature of 1. At the beginning of each trial, the SSM's hidden states are initialized to zero.

Throughout our experiments, we employed the actor with 1 neuron and a critic with 1 neuron fully connected to the SSM output. The list of hyperparameters has been summarized in Table 1.

During training, the actor updates its policy in the direction suggested by the critic, using the temporal-difference (TD) error based on the discounted cumulative reward, which captures both immediate and future rewards with a decay factor, as a learning signal. On the other hand, the critic minimizes the TD error to improve the accuracy of its value estimates. This cooperative interaction enables stable and efficient policy learning. During inference, only the actor is used to generate actions, as the critic is not required once the policy has been learned. In particular, the final action is sampled based on the probability of selecting an action predicted by the policy network.

Parameter Name	Value	Note
Learning Rate	3e-4	Weight update speed
Weight Decay	1e-6	Regularization
Training Episodes	250000	Total trials
Batch size	1	Only 1 trial at a time
Optimizer	Adam	Default PyTorch Adam
<b>SSM Hyperparameters</b>		
Neurons	50~80	Depending on the task
Discretization	Zero-Order Hold (ZOH)	Default S5 discretization
Dropout Rate	0.1	Regularization
Initialization	HiPPO	S5 Initialization
Surrogate Function	Sigmoid	Most smooth surrogation
<b>RL Hyperparameters</b>		
Policy Agent Neuron	1	Makes prediction/action
Critic Network Neuron	1	Estimates state reward
Reward Discount Factor	0.99	Dampens reward expectation
Initial Entropy	0.3	Linearly decays to 0 over trial

**Table 1:** Hyperparameters used in experiments

## Reference

1. Jun, J. J. *et al.* Fully integrated silicon probes for high-density recording of neural activity. *Nature* **551**, 232–236 (2017).
2. Stringer, C. *et al.* Spontaneous behaviors drive multidimensional, brainwide activity. *Science* **364**, eaav7893 (2019).
3. Bassett, D. S. & Sporns, O. Network neuroscience. *Nat Neurosci* **20**, 353–364 (2017).
4. Ivry, R. B. & Spencer, R. M. The neural representation of time. *Current Opinion in Neurobiology* **14**, 225–232 (2004).
5. Pastalkova, E., Itskov, V., Amarasingham, A. & Buzsáki, G. Internally generated cell assembly sequences in the rat hippocampus. *Science* **321**, 1322–1327 (2008).
6. Salz, D. M. *et al.* Time Cells in Hippocampal Area CA3. *J. Neurosci.* **36**, 7476–7484 (2016).
7. Eichenbaum, H. Time cells in the hippocampus: a new dimension for mapping memories. *Nat Rev Neurosci* **15**, 732–744 (2014).
8. Toso, A., Reinartz, S., Pulecchi, F. & Diamond, M. E. Time coding in rat dorsolateral striatum. *Neuron* **109**, 3663-3673.e6 (2021).
9. Matell, M. S. & Meck, W. H. Cortico-striatal circuits and interval timing: coincidence detection of oscillatory processes. *Cognitive Brain Research* **21**, 139–170 (2004).
10. Hodgkin, A. L. & Huxley, A. F. A quantitative description of membrane current and its application to conduction and excitation in nerve. *J Physiol* **117**, 500–544 (1952).
11. Izhikevich, E. M. Which model to use for cortical spiking neurons? *IEEE Transactions on Neural Networks* **15**, 1063–1070 (2004).
12. Herz, A. V. M., Gollisch, T., Machens, C. K. & Jaeger, D. Modeling Single-Neuron Dynamics and Computations: A Balance of Detail and Abstraction. *Science* **314**, 80–85 (2006).
13. Liboni, L. H. B. *et al.* Image segmentation with traveling waves in an exactly solvable recurrent neural network. *Proceedings of the National Academy of Sciences* **122**,

e2321319121 (2025).

14. Lu, S. & Sengupta, A. Deep unsupervised learning using spike-timing-dependent plasticity. *Neuromorph. Comput. Eng.* **4**, 024004 (2024).
15. Muller, L., Churchland, P. S. & Sejnowski, T. J. Transformers and cortical waves: encoders for pulling in context across time. *Trends in Neurosciences* **47**, 788–802 (2024).
16. Zhou, S., Seay, M., Taxidis, J., Golshani, P. & Buonomano, D. V. Multiplexing working memory and time in the trajectories of neural networks. *Nat Hum Behav* **7**, 1170–1184 (2023).
17. Lin, D., Huang, A. Z. & Richards, B. A. Temporal encoding in deep reinforcement learning agents. *Sci Rep* **13**, 22335 (2023).
18. Taxidis, J. *et al.* Differential Emergence and Stability of Sensory and Temporal Representations in Context-Specific Hippocampal Sequences. *Neuron* **108**, 984-998.e9 (2020).
19. Zador, A. M. A critique of pure learning and what artificial neural networks can learn from animal brains. *Nat Commun* **10**, 3770 (2019).
20. Heys, J. G. & Dombeck, D. A. Evidence for a subcircuit in medial entorhinal cortex representing elapsed time during immobility. *Nat Neurosci* **21**, 1574–1582 (2018).
21. van der Molen, T. *et al.* Preconfigured neuronal firing sequences in human brain organoids. *Nat Neurosci* 1–13 (2025) doi:10.1038/s41593-025-02111-0.
22. Gu, A. & Dao, T. Mamba: Linear-Time Sequence Modeling with Selective State Spaces. Preprint at <http://arxiv.org/abs/2312.00752> (2024).
23. Yang, S., Wang, B., Shen, Y., Panda, R. & Kim, Y. Gated Linear Attention Transformers with Hardware-Efficient Training. Preprint at <https://doi.org/10.48550/arXiv.2312.06635> (2024).
24. Gu, A., Dao, T., Ermon, S., Rudra, A. & Re, C. HiPPO: Recurrent Memory with Optimal Polynomial Projections. Preprint at <https://doi.org/10.48550/arXiv.2008.07669> (2020).

25. Smith, J. T. H., Warrington, A. & Linderman, S. W. Simplified State Space Layers for Sequence Modeling. Preprint at <https://doi.org/10.48550/arXiv.2208.04933> (2023).

26. Gu, A., Dao, T., Ermon, S., Rudra, A. & Ré, C. HiPPO: Recurrent Memory with Optimal Polynomial Projections. in *Advances in Neural Information Processing Systems* vol. 33 1474–1487 (Curran Associates, Inc., 2020).

27. Dragoi, G. & Tonegawa, S. Selection of preconfigured cell assemblies for representation of novel spatial experiences. *Philos Trans R Soc Lond B Biol Sci* **369**, 20120522 (2014).

28. Soares, S., Atallah, B. V. & Paton, J. J. Midbrain dopamine neurons control judgment of time. *Science* **354**, 1273–1277 (2016).

29. Gu, A., Goel, K., Gupta, A. & Ré, C. On the Parameterization and Initialization of Diagonal State Space Models. *Advances in Neural Information Processing Systems* **35**, 35971–35983 (2022).

30. Churchland, M. M. et al. Neural population dynamics during reaching. *Nature* **487**, 51–56 (2012).

31. Gallego, J. A., Perich, M. G., Miller, L. E. & Solla, S. A. Neural Manifolds for the Control of Movement. *Neuron* **94**, 978–984 (2017).

32. Khona, M. & Fiete, I. R. Attractor and integrator networks in the brain. *Nat Rev Neurosci* **23**, 744–766 (2022).

33. Mello, G. B. M., Soares, S. & Paton, J. J. A Scalable Population Code for Time in the Striatum. *Current Biology* **25**, 1113–1122 (2015).

34. Wang, J., Narain, D., Hosseini, E. A. & Jazayeri, M. Flexible timing by temporal scaling of cortical responses. *Nat Neurosci* **21**, 102–110 (2018).

35. Sun, C., Yang, W., Martin, J. & Tonegawa, S. Hippocampal neurons represent events as transferable units of experience. *Nat Neurosci* **23**, 651–663 (2020).

36. Cadena-Valencia, J., García-Garibay, O., Merchant, H., Jazayeri, M. & de Lafuente, V. Entrainment and maintenance of an internal metronome in supplementary motor area. *eLife*

7, e38983 (2018).

37. Gámez, J., Mendoza, G., Prado, L., Betancourt, A. & Merchant, H. The amplitude in periodic neural state trajectories underlies the tempo of rhythmic tapping. *PLOS Biology* **17**, e3000054 (2019).

38. Betancourt, A., Pérez, O., Gámez, J., Mendoza, G. & Merchant, H. Amodal population clock in the primate medial premotor system for rhythmic tapping. *Cell Reports* **42**, (2023).

39. Izhikevich, E. M. *Dynamical Systems in Neuroscience*. (MIT Press, 2007).

40. Paton, J. J. & Buonomano, D. V. The Neural Basis of Timing: Distributed Mechanisms for Diverse Functions. *Neuron* **98**, 687–705 (2018).

41. Tsao, A., Yousefzadeh, S. A., Meck, W. H., Moser, M.-B. & Moser, E. I. The neural bases for timing of durations. *Nat Rev Neurosci* **23**, 646–665 (2022).

42. Sánchez-Moncada, I., Concha, L. & Merchant, H. Pre-supplementary Motor Cortex Mediates Learning Transfer from Perceptual to Motor Timing. *J. Neurosci.* **44**, (2024).

43. Finn, C., Abbeel, P. & Levine, S. Model-Agnostic Meta-Learning for Fast Adaptation of Deep Networks. in *Proceedings of the 34th International Conference on Machine Learning* 1126–1135 (PMLR, 2017).

44. Hospedales, T., Antoniou, A., Micaelli, P. & Storkey, A. Meta-Learning in Neural Networks: A Survey. *IEEE Transactions on Pattern Analysis and Machine Intelligence* **44**, 5149–5169 (2022).

45. Shikano, Y., Ikegaya, Y. & Sasaki, T. Minute-encoding neurons in hippocampal-striatal circuits. *Curr Biol* **31**, 1438-1449.e6 (2021).

46. Skaggs, W. E. & McNaughton, B. L. Replay of Neuronal Firing Sequences in Rat Hippocampus During Sleep Following Spatial Experience. *Science* **271**, 1870–1873 (1996).